AMERICAN SOCIETY FOR MICROBIOLOGY | Applied and Environmental Microbiology

# Physiological and Proteomic Responses of Continuous Cultures of *Microcystis aeruginosa* PCC 7806 to Changes in Iron Bioavailability and Growth Rate

**Anna C. Y. Yeung,[a,b] Paul M. D'Agostino,[b,c] Anne Poljak,[d] James McDonald,[a] Mark W. Bligh,[a] T. David Waite,[a] Brett A. Neilan[b]**

School of Civil and Environmental Engineering, UNSW, Sydney, NSW, Australia[a]; School of Biomolecular and Biosciences, UNSW, Sydney, NSW, Australia[b]; Department of Chemistry, Technische Universität München, Garching, Bayern, Germany[c]; Bioanalytical Mass Spectrometry Facility, UNSW, Sydney, NSW, Australia[d]

**ABSTRACT**

**The hepatotoxin microcystin (MCYST) is produced by a variety of freshwater cyanobacterial species, including *Microcystis aeruginosa*. Interestingly, MCYST-producing *M. aeruginosa* strains have been shown to outcompete their nontoxic counterparts under iron-limiting conditions. However, the reasons for this are unclear. Here we examined the proteomic response of *M. aeruginosa* PCC 7806 continuous cultures under different iron and growth regimes. Iron limitation was correlated with a global reduction in levels of proteins associated with energy metabolism and photosynthesis. These proteomic changes were consistent with physiological observations, including reduced chlorophyll *a* content and reduced cell size. While levels of MCYST biosynthesis proteins did not fluctuate during the study period, both intra- and extracellular toxin quotas were significantly higher under iron-limiting conditions. Our results support the hypothesis that intracellular MCYST plays a role in protecting the cell against oxidative stress. Further, we propose that extracellular MCYST may act as a signaling molecule, stimulating MCYST production under conditions of iron limitation and enhancing the fitness of bloom populations.**

**IMPORTANCE**

**Microcystin production in water supply reservoirs is a global public health problem. Understanding the ecophysiology of hepatotoxic cyanobacteria, including their responses to the presence of key micronutrient metals such as iron, is central to managing harmful blooms. To our knowledge, this was the first study to examine proteomic and physiological changes occurring in *M. aeruginosa* continuous cultures under conditions of iron limitation at different growth rates.**

Cyanobacteria ("blue-green algae") proliferate in warm stratified water bodies rich in nitrogen and phosphorus (1, 2). Cyanobacterial blooms can have a negative impact on the appearance, taste, and odor of water, and their subsequent decay can lead to oxygen depletion and fish kills (3). However, of greatest concern to public health is their production of potent toxins. *Microcystis aeruginosa* (Kützing) Lemmermann is a common bloom-forming cyanobacterial species that produces hepatotoxic microcystins (MCYSTs) (1). These nonribosomally synthesized peptides inhibit eukaryotic protein phosphatases, leading to liver necrosis in acute doses and hepatocellular carcinoma in chronic low doses (4, 5).

There is strong evidence that the production of MCYST is a direct function of cell division (6). It is therefore not surprising that parameters affecting cyanobacterial growth rate (e.g., nutrients, trace metals, temperature, pH, and light) have been correlated with fluctuating MCYST levels in batch culture experiments (7–9).

Recent molecular studies suggest that iron (Fe) and nitrogen (N) also play a role in regulating the expression of MCYST biosynthesis (*mcy*) genes. In *M. aeruginosa*, for example, the *mcy* promoter region contains binding sites for the ferric uptake regulator (Fur) and the global nitrogen regulator (NtcA) (10, 11). Despite these genetic clues, the metabolism of MCYST in cyanobacteria is poorly understood. Likewise, the physiological role of the toxin is unknown, although several theories have been proposed.

A pivotal study by Zilliges et al. (12) suggested that MCYST may protect the cell against oxidative stress by binding to cysteine residues on redox-sensitive proteins, effectively blocking attack by reactive oxygen species (ROS). In line with this, MCYST cell quotas have been observed to increase under conditions that favor the generation of ROS, including Fe limitation (13). Fe bioavailability is generally low in most aqueous environments given the relatively rapid oxidation of the more soluble ferrous form [Fe(II)] into the thermodynamically stable and highly insoluble ferric form [Fe(III)] at circumneutral pH (14, 15). In addition, natural organic matter such as fulvic and humic acids can bind Fe, thereby rendering it unavailable (16).

Cyanobacteria have a higher Fe requirement than most other microorganisms (17), as that micronutrient is crucial for specific cellular processes, including photosynthetic electron transport, nitrogen fixation, and pigment production, and for various transcription and translational processes (17, 18). During the summer period, bioavailable Fe levels can deplete quickly as cyanobacteria

**Received** 19 April 2016 **Accepted** 24 July 2016

**Accepted manuscript posted online** 29 July 2016

**Citation** Yeung ACY, D'Agostino PM, Poljak A, McDonald J, Bligh MW, Waite TD, Neilan BA. 2016. Physiological and proteomic responses of continuous cultures of *Microcystis aeruginosa* PCC 7806 to changes in iron bioavailability and growth rate. Appl Environ Microbiol 82:5918–5929. doi:10.1128/AEM.01207-16.

**Editor:** R. M. Kelly, North Carolina State University

Address correspondence to Brett A. Neilan, b.neilan@unsw.edu.au.

Supplemental material for this article may be found at http://dx.doi.org/10.1128/AEM.01207-16.

(and other phytoplankton) grow rapidly (19). Limiting the availability of this crucial micronutrient, along with high light stress, often leads to a phenomenon called photosystem decoupling, where production of excess electrons in the photosynthetic chain without oxygen evolution results in oxidative damage and chlorosis (20, 21). Fe starvation has been shown to result in oxidative stress in several MCYST-producing cyanobacterial genera, including *Microcystis* (22), *Anabaena* (23), and *Nostoc* (24).

Under normal conditions, cyanobacteria avoid accumulation of reduced iron [Fe(II)] and $H_2O_2$ by activating Fe storage proteins (e.g., bacterioferritin) and ROS-regulating enzymes such as superoxide dismutase (SOD) and peroxidases (25, 26). Under stress conditions (including primary and trace nutrient depletion), however, excess electrons from unbalanced electron flow can lead to the formation of ROS which break down Fe-centered enzymes, leading to the release of Fe(II) (23). Reduced iron and $H_2O_2$ can accumulate and initiate the Fenton reaction by which Fe(II) reacts with $H_2O_2$, producing strongly oxidizing species, such as the hydroxyl radical (·OH), and leading to oxidative stress (25, 27).

There is an increasing consensus that MCYST production represents a response to oxidative stress, with this large molecule binding to cysteine residues to protect proteins from ROS attack (12). Also, MCYST is capable of effectively scavenging ·OH (28, 29), though little is known of the impact that the resultant degradation products might have on cell growth or viability.

In order to better understand the relationships among Fe status, oxidative stress, and MCYST production in hepatotoxic cyanobacteria, we investigated the proteomic profiles of *M. aeruginosa* PCC 7806 continuous cultures under Fe-limited and Fe-replete conditions at different growth rates. The results suggest that the global proteomic responses to Fe limitation in *M. aeruginosa* consist of downregulation of photosynthesis and energy metabolism proteins and upregulation of transporter proteins with a concomitant increase in MCYST production. These results are discussed with respect to the ecophysiology of *M. aeruginosa*.

## MATERIALS AND METHODS

**Cyanobacterial continuous culturing conditions.** *M. aeruginosa* PCC 7806 was acquired from The Pasteur Culture Collection and maintained in BG11 medium. Cultures were incubated with agitation at 27°C under conditions of photon irradiance of 157 μmol photons (photosynthetically active radiation [PAR]) $m^{-2}$ $s^{-1}$ with a 14-h/10-h light-to-dark cycle. Cultures were transferred to nutrient-replete Fraquil* medium (a medium in which the chemical identification of species of trace metals is well defined and which is therefore suitable for the investigation of cellular responses to trace metal availability) (30). Since concentrations of some major nutrients, including nitrate, are relatively low in original Fraquil* medium, a nutrient-replete Fraquil* medium, with which optimal cellular growth is achieved, was developed by modifying the major nutrient concentrations to levels equivalent to those present in BG11 medium (referred to as Fraquil*BG11) (M. Fujii, unpublished data). Cells were acclimated to Fraquil*BG11 for two generations before the commencement of the Fe limitation experiment.

The chemostat system employed was developed in a previous study (31). All culture vessels and plumbing were constructed from metal-free materials. Under steady-state conditions, the dilution rate (D) was equal to the specific growth rate (μ) with D set to 0.07 $day^{-1}$, 0.15 $day^{-1}$, 0.30 $day^{-1}$, and 0.45 $day^{-1}$ by adjusting the diameter of the feed tubes (31). The Fe concentrations in Fraquil*BG11 were the same as those described in reference 13, i.e., 100 nM (Fe-limited conditions) and 1,000 nM (Fe-replete conditions). Continuous cultures were set up in triplicate and maintained until cells reached and remained at the steady state for seven consecutive samplings (as determined by manual cell counting and chlorophyll [Chl] extract measurements). Cultures were harvested at day 40 for Fe-limited and day 42 for Fe-replete cultures for subsequent physiological analyses and cell counts (using a manual hemocytometer). Cell size was determined using a light microscope (Leica) calibrated with 5-μm-diameter beads using imagining software (Leica Microsystems). The chlorophyll *a* (Chl *a*) content of cultures was estimated according to the method described in reference 32. Briefly, Chl *a* was extracted from 2 ml culture using methanol and the absorbance at 665 nm ($A_{665}$) measured. The concentration of Chl *a* (expressed in micrograms per milliliter) was calculated by multiplying the $A_{665}$ by 12.7 (the Chl *a* extinction coefficient). The remainder of the culture was sacrificed for the proteomic experiments.

**Microcystin extraction and quantification.** Two milliliters of steady-state culture was harvested via centrifugation (14,000 × *g*, 10 min). The supernatant was removed for subsequent analysis of extracellular MCYST ($MCYST_{ext}$) levels via liquid chromatography-tandem mass spectrometry (LC-MS/MS; see below). Intracellular MCYST ($MCYST_{int}$) was extracted by resuspending the cell pellet in 80% (vol/vol) aqueous methanol and disrupting the cells twice for 30 s each time in a FastPrep FP120 cell disrupter (Qbiogene Inc.) at top speed using 0.5-mm-diameter zirconium silicate beads. Cell debris and beads were removed by centrifugation (14,000 × *g*, 10 min), and the supernatant was evaporated in a Savant SpeedVac SC110 concentrator. As an additional purification step, 500 μl of 40% (vol/vol) aqueous methanol and 500 μl of 40% (vol/vol) chloroform were added to the samples and the tubes were incubated for 3 min with shaking and then centrifuged (12,000 × *g*, 15 min) to separate the aqueous methanol and chloroform. The aqueous layer was removed for subsequent analysis via LC-MS/MS performed with a suite of MCYST standards (Enzo Life Sciences; see Table S1 in the supplemental material). Solutions of each target MCYST were prepared in 100% high-performance-LC (HPLC)-grade methanol. Fraquil*BG11 medium and 40% aqueous methanol were used as blank control matrices.

LC-MS/MS was performed on an Agilent 1200 LC instrument (Agilent Technologies) fitted with a Phenomenex Luna column (5-μm pore size; 150 by 4.6 mm) and a $C_{18}$ column guard (Torrance) (5-μm pore size; 4 by 2 mm). The column oven temperature was kept at 30°C. The mobile phases used were composed of 0.1% formic acid–water (mobile phase A) and 0.1% formic acid–acetonitrile (mobile phase B). Mobile phase A was held at 95% for 5 min to equilibrate the system until the initial conditions were set. The gradient run was from 5% mobile phase B to 85% mobile phase B over 21 min and then back to 5% mobile phase B for 2 min, delivered at a flow rate of 800 μl/min. The mobile phase gradient is described in Table S2 in the supplemental material. The sample injection volume was 20 μl. An Applied Biosystem API 4000 Q Trap spectrometer equipped with a Turbo V source and an electrospray ionization (ESI) probe was used for MCYST detection in positive polarity.

For each target MCYST, the three most intense multiple reaction monitoring (MRM) transitions were determined using direct infusion of each target MCYST into a Turbo V ion source. The most intense MRM transition was used to quantify the concentration of the analyte, while the less intense MRM transitions were used for qualitative confirmation. The elution times (retention times [RT]) and MRM transitions for MCYST standards are summarized in Table S1 in the supplemental material. The operating parameters of the MS/MS were optimized by flow injection analysis, with optimal values summarized in Table S3. Quantification of all target compounds was achieved using a 5-point calibration curve with linearity $r^2$ values of >0.99 and a range of 1 to 200 ng/ml. Method reporting limits were determined as the lowest concentration of an injected MCYST standard affording a peak with a signal-to-noise ratio greater than 5. Microcystin measurements were normalized to cell number to give total MCYST quotas ($Q_{MCYST}$) equivalent to the sum of $MCYST_{int}$ (intracellular MCYST) and $MCYST_{ext}$ (MCYST in the extracellular medium). All LC-MS/MS results are presented as mean values of results from three

replicate cultures for each dilution condition. All data were analyzed by one-way analysis of variance (ANOVA). Once a significant difference was detected, *post hoc* multiple comparisons were performed using the Tukey method. The level of significance was set at 0.05 for all tests.

**Oxidative stress measurements.** To measure oxidative stress, $H_2$DCFDA (2′,7′-dichlorodihydrofluorescein diacetate) was used as a probe to detect the presence of reactive oxygen species (ROS) within the cells. The dye permeates the cell wall, with cellular esterases subsequently hydrolyzing the diacetate bond to form the stable but nonfluorescent compound $H_2$DCF (2′,7′-dichlorodihydrofluorescein). This compound reacts with intracellular ROS to form the highly fluorescent compound DCF (2′,7′-dichlorofluorescein). Stock solutions of $H_2$DCFDA (10 mM) were prepared in dimethyl sulfoxide (DMSO) to enhance penetration through the cell membrane (33). Approximately $0.5 \times 10^7$ to $1 \times 10^7$ cells were collected under each set of Fe and dilution rate conditions. Cells were washed with fresh Fraquil*BG11 and then resuspended in 1 ml of the same medium supplemented with 25 μM $H_2$DCFDA. Samples were wrapped in foil and incubated with shaking for 1 h at 25°C to allow dye absorption. Cells were then harvested via centrifugation (14,000 × *g*, 10 min) and resuspended in fresh Fraquil*BG11 to remove unabsorbed dye. The fluorescence emitted by $5 \times 10^5$ cells was measured using a BD FACSAria II cell sorter flow cytometer (BD Biosciences), using excitation and emission filters with wavelengths of 450 and 530 nm, respectively.

Following initial fluorescence measurements, hydrogen peroxide ($H_2O_2$) was added to cells to examine their response to $H_2O_2$-induced oxidative stress. An aliquot of 500 μl of each sample was transferred into a fresh tube and 4 mM $H_2O_2$ was added, and the contents of the tube were mixed briefly and then incubated for 10 to 30 min at ambient room temperature and the tube was covered with foil. Fluorescence was measured as previously described.

**Protein extraction.** Proteins were extracted from each replicate culture as follows. Seventy milliliters of culture was harvested by centrifugation (5,000 × *g*, 15 min, 20°C). The cell pellet was washed with fresh medium and resuspended in 500 μl of extraction buffer (50 mM HEPES [pH 7.0], 0.1% SDS, 0.01% Triton X-100, MilliQ water) (34) supplemented with 1 mM protease inhibitor (phenylmethylsulfonyl fluoride [PMSF]). Cells were partially lysed using three freeze-thaw cycles, alternating submersion in liquid nitrogen and warm water (37°C). The lysate was sonicated on ice using a Branson Sonifier (25% amplitude, 3 sonication procedures performed for 30 s each). Cell extracts were centrifuged (14,000 × *g*, 10 min, 20°C), and the supernatant was transferred to a clean 1.5-ml polypropylene tube. The cell pellet was extracted again as previously described. Supernatant fractions were combined, and biological triplicates were pooled for precipitation with 9 volumes of ice-cold acetone (4°C, overnight). Protein pellets were air-dried and resuspended in dissolving buffer (50 mM $NaHCO_3$, 0.08% SDS, MilliQ water) for quantification via the bicinchoninic acid (BCA) assay. A portion (15 μg) of each sample was separated by SDS-PAGE (NuPAGE 4% to 12% Bis-Tris gradient gels; Invitrogen) and visualized by colloidal Coomassie staining (35).

**iTRAQ labeling and sample cleanup.** Two individual 4-plex experiments using isobaric tags for relative and absolute quantitation (iTRAQ) were conducted corresponding to Fe-limited (iTRAQ-low) and Fe-replete (iTRAQ-high) chemostat experiments (see Fig. S3 in the supplemental material). iTRAQ labeling was carried out using the manufacturer's instructions and a previously published approach (36). In brief, 100 μg of protein was reduced using 2 mM Tris-(2-carboxyethyl) phosphine (TCEP; 60°C, 1 h) and alkylated with 2 mM iodoacetamide (ambient temperature, 10 min). Proteins were then digested overnight with trypsin (~18 h). Immediately prior to the addition of iTRAQ reagents, 1 μl $Na_2CO_3$ (500 mM) was added to ensure a basic pH (~8.5). The iTRAQ labels were each resuspended in 70 μl of isopropanol. Each chemostat dilution rate, 0.07 $day^{-1}$, 0.15 $day^{-1}$, 0.30 $day^{-1}$, or 0.45 $day^{-1}$, had a unique iTRAQ label of 114, 115, 116, or 117, respectively. Samples were incubated with the iTRAQ labels at ambient temperature for 1 h, after which time the labeled samples were combined.

The combined labeled peptide mixture was passed through a cation exchange column (Applied Biosystems) to remove excess reagents and detergent. Following the off-line strong-cation exchange, the labeled peptides were dried under vacuum and resuspended in 500 μl of 0.2% heptafluorobutyric acid (HFBA)–water. The sample was passed through an off-line $C_{18}$ desalting cartridge (Peptide MacroTrap; Michrom Bioresources) and eluted with 500 μl $CH_3CN$–water–formic acid (50:50:0.1 [vol/vol/vol]) followed by 200 μl neat $CH_3CN$. The resulting eluent was dried and the pellet dissolved in 0.05% HFBA–0.1% formic acid (400 μl).

**Mass spectrometry and data analysis.** Two-dimensional (2D) LC-MS/MS mass spectrometry was performed on an API QStar Elite hybrid tandem mass spectrometer (Applied Biosystems). Peptides (3 to 5 μg total load) were initially captured onto a SCX microcolumn (Poros S10; Applied Biosystems) (0.75 by ~20 mm), and the eluant from multiple salt elution steps (unbound load and 5, 10, 15, 20, 25, 30, 40, 50, 100, 250, 500, and 1,000 mM ammonium acetate) was captured and desalted on a $C_{18}$ precolumn cartridge (Michrom Bioresources) (500 μm by 2 mm). After a 10-min wash, the precolumn was switched (Switchos) into line with a fritless analytical column (75 μm by 12 cm) containing $C_{18}$ reverse-phase packing material (Magic) (5 μm, 200Å) (37). Peptides were eluted using a 90-min gradient of buffer A (2% [vol/vol] $CH_3CN$, 0.1% formic acid) to buffer B (80% [vol/vol] $CH_3CN$, 0.1% formic acid) at ~300 ml/min. An electric current (2,300 V) was applied through a low-volume tee (Upchurch Scientific) at the column inlet, and the outlet was positioned ~1 cm from the orifice of the mass spectrometer. Positive ions were generated by electrospray and the QStar operated in information-dependent acquisition (IDA) mode. A time of flight (TOF) MS survey scan was acquired (*m/z* 350 to 1,700, 0.75 s), and the three largest multiply charged ions (counts, >20; charge state, +2 to +4) were sequentially selected by Q1 for MS/MS analysis. Nitrogen was used as collision gas, and an optimum collision energy value was automatically chosen (based on charge state and mass). Tandem mass spectra were accumulated for up to 2.5 s (*m/z* 65 to 2,000) with two repeats. Automated online 2D LC-MS/MS was carried out (with two technical replicates for each iTRAQ study), and the combined data were processed using ProteinPilot V 4.5 software (ABSciex) against a database library comprised of available *M. aeruginosa* protein sequences from NCBI (downloaded February 2014). A *P* value of <0.05 was used as the cutoff for accepting statistically significant changes in protein expression levels. False-discovery-rate (FDR) reports were generated using a detected-protein threshold of greater than 1.00 (equivalent to a 90% confidence level) and a ProtScore of 2.00. The mass spectrometry proteomics data were deposited into the ProteomeXchange Consortium (38) via the PRIDE partner repository with the data set identifier PXD002930.

## RESULTS

**Steady-state physiological differences.** The growth of MCYST-producing *M. aeruginosa* in Fe-limited (100 nM) and Fe-replete (1,000 nM) chemostats was monitored over 40 and 42 days, respectively (see Fig. S1 in the supplemental material). Both Fe conditions supported maximum cell concentrations at the lowest dilution rate (0.07 $day^{-1}$); however, the growth supported under Fe-replete conditions (~$1.7 \times 10^{11}$ cells $liter^{-1}$) was denser than that supported under Fe-limited conditions (~$3.2 \times 10^{10}$ cells $liter^{-1}$) (see Fig. S1). Chlorophyll content was constant across the dilution rates for Fe-limited cultures; however, it decreased with lower dilution rates for Fe-replete cultures (Table 1). Conversely, cell diameter increased with decreasing dilution rates regardless of Fe conditions, likely as a result of cells having more time to grow before cell division or before being washed out (Table 1). Chlorosis was not evident by visual inspection, although the chlorophyll quotas in the cultures were lower under Fe-limited conditions

**TABLE 1** Summary of physiological characteristics of cells from Fe-limited and Fe-replete chemostats[a]

| Dilution rate ($day^{-1}$) | Values under indicated chemostat conditions | | | | | |
|---|---|---|---|---|---|---|
| | Chl *a* (pg per 100 cells) | | Cell size (μm) | | $Q_{MCYST}$ ($fg\ cell^{-1}$) | |
| | Fe limited | Fe replete | Fe limited | Fe replete | Fe limited | Fe replete |
| 0.07 | 0.04 ± 0.02 | 0.10 ± 0.04 | 4.01 ± 0.03 | 4.35 ± 0.10 | Tot, 63.34; Int, 59.24; Ext, 4.10 | Tot, 41.39; Int, 41.39; Ext, ND |
| 0.15 | 0.04 ± 0.02 | 0.20 ± 0.05 | 4.04 ± 0.05 | 4.27 ± 0.06 | Tot, 57.27; Int, 55.63; Ext, 1.64 | Tot, 41.52; Int, 41.52; Ext, ND |
| 0.30 | 0.04 ± 0.03 | 0.40 ± 0.13 | 3.94 ± 0.07 | 4.15 ± 0.16 | Tot, 66.93; Int, 65.54; Ext, 1.39 | Tot, 22.71; Int, 22.71; Ext, ND |
| 0.45 | 0.04 ± 0.01 | 0.60 ± 0.05 | 3.89 ± 0.09 | 4.08 ± 0.03 | Tot, 62.50; Int, 60.97; Ext, 1.53 | Tot, 17.90; Int, 17.90; Ext, ND |

[a] Tot, total; Int, intracellular; Ext, extracellular; ND, not detected.

than under Fe-replete conditions; the cells were also smaller under Fe-limited conditions than under Fe-replete conditions.

**Microcystin analysis.** Microcystin-LR and [D-Asp3]MCYST-LR were the only MCYST variants detected in *M. aeruginosa* PCC 7806, concurring with a previous report by Tonk et al. (39). The $Q_{MCYST}$ data are presented in Table 1. In Fe-replete cultures, there was a trend for higher $Q_{MCYST}$ levels at lower dilution rates, with the results ranging from a minimum of 17.9 ± 1.1 fg $cell^{-1}$ at 0.45 $day^{-1}$ to a maximum of 41.4 ± 6.3 fg $cell^{-1}$ at 0.07 $day^{-1}$. In comparison, $Q_{MCYST}$ values were similar across the dilution rates for Fe-limited cultures and averaged 62.5 ± 4.0 fg $cell^{-1}$. Overall, $Q_{MCYST}$ values were higher for Fe-limited cultures than for Fe-replete cultures across all dilution rates and were significantly higher than those seen with Fe-replete cultures at dilution rates of 0.45 $day^{-1}$ (3.5-fold, unpaired *t* test, $n = 3$, $P < 0.05$) and 0.30 $day^{-1}$ (2.5-fold, unpaired *t* test, $n = 3$, $P < 0.05$) (Fig. 1A). Under Fe-replete conditions, $MCYST_{int}$ values were highest in cultures grown at the lower dilution rates, with MCYST-LR making up 80% of the intracellular MCYST content. Extracellular MCYST was not detected in any of the Fe-replete cultures (Fig. 1B). In contrast, in the Fe-limited cultures, $MCYST_{int}$ quotas were similar across all dilution rates, with [D-Asp3]MCYST-LR making up approximately 34% of the intracellular MCYST content (Fig. 1C). Both MCYST variants were also observed in the extracellular fraction of Fe-limited cultures, with the $MCYST_{ext}$ values measured at the 0.07 $day^{-1}$ dilution rate ($P < 0.0001$) being significantly higher than those measured at the other dilution rates (Fig. 1D). Extracellular MCYST-LR and [D-Asp3]MCYST-LR were detected in approximately equal proportions in Fe-limited cultures.

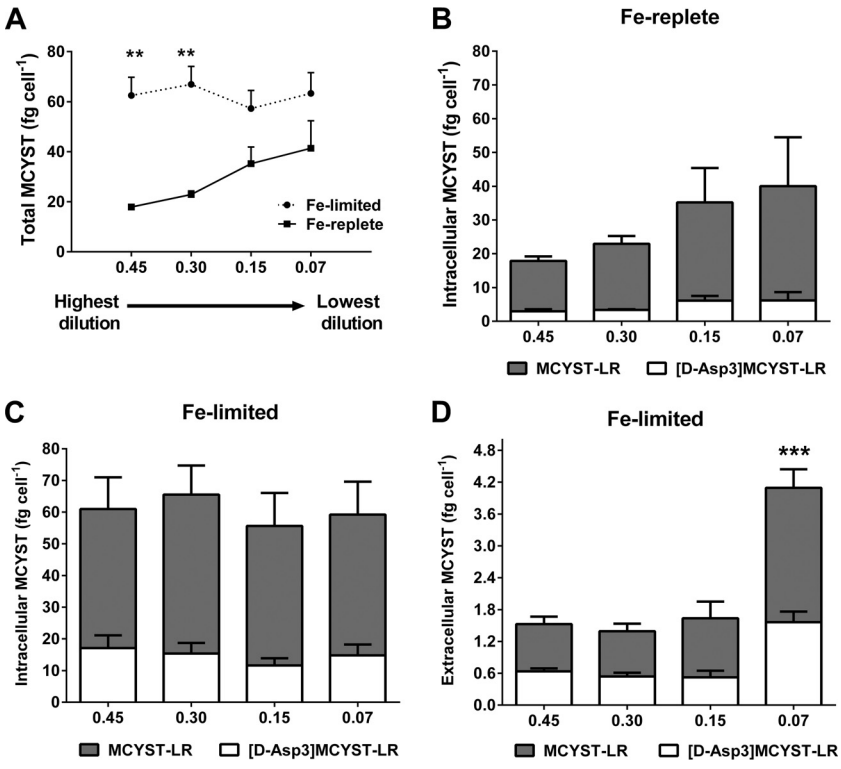


**FIG 1** LC/MS analyses of microcystin from Fe-limited and Fe-replete chemostats. (A) Total MCYST quotas ($Q_{MCYST}$) in Fe-limited and Fe-replete chemostats. (B) Intracellular MCYST from Fe-replete cultures. (C) Intracellular MCYST from Fe-limited cultures. (D) Extracellular MCYST from Fe-limited cultures. For graphs B to D, shaded columns represent MCYST-LR and unshaded columns represent [D-Asp3]MCYST-LR. Error bars indicate standard deviation from biological triplicates. Extracellular MCYST was not detected in Fe-replete cultures. Asterisks indicate statistical significance after performing multiple-comparison tests between data for Fe-limited and Fe-replete cultures. *X*-axis numbers represent dilution rates per day.

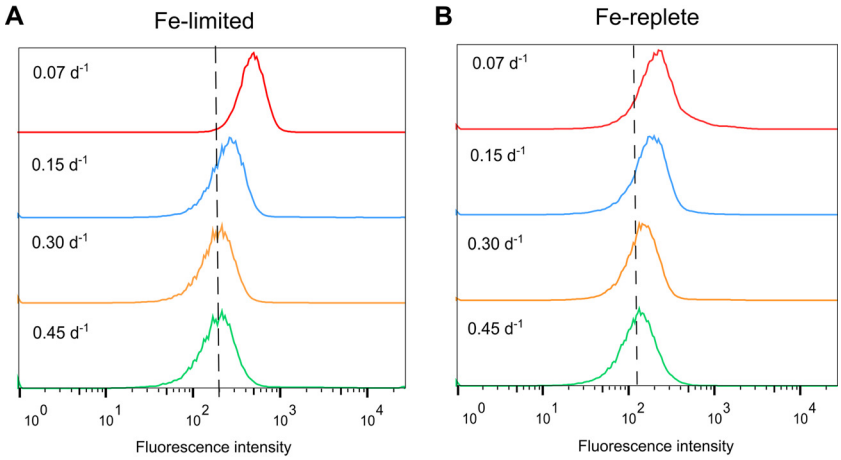


**FIG 2** Oxidative stress in (A) Fe-limited cultures and (B) Fe-replete cultures as detected by the fluorescence-based assay for reactive oxygen species (ROS). Fluorescein diacetate ($H_2$DCFDA) was used to detect intracellular ROS in cells grown at different dilution rates. Increased levels of ROS are indicated by shifts to the right along the *x* axis. Histograms are arranged according to increasing dilution rates, with the lowest dilution rate (0.07 per day [$d^{-1}$]) at the top and the highest dilution rate (0.45 $d^{-1}$) at the bottom.

**Production of ROS.** Iron limitation interrupts photosynthetic processes, leading to the generation of excess ROS, which damage DNA, RNA, and proteins (23). The results of our fluorescence-based assay for ROS demonstrated that Fe-limited cultures produced higher levels of ROS than Fe-replete cultures (Fig. 2). Oxidative stress was also correlated to growth rate in Fe-limited cultures, with cells grown at the low (0.07 $day^{-1}$) dilution rate producing markedly greater levels of ROS than those grown at higher dilution rates (Fig. 2A). In comparison, fluctuations in ROS levels were minimal in Fe-replete cultures regardless of the dilution rate (Fig. 2B).

The responses of *M. aeruginosa* cultures to $H_2O_2$-induced oxidative stress also differed between the Fe treatments. Cells from Fe-limited cultures grown at the 0.07 $day^{-1}$ dilution rate exhibited the strongest fluorescence shift during the course of the incubation (Fig. 3A), followed by those grown at the 0.15 $day^{-1}$ rate (Fig. 3B). However, fluorescence changes were not observed for Fe-limited cultures grown at the higher dilution rates (Fig. 3C and D). Interestingly, all Fe-replete cultures exhibited increased fluorescence shifts after the addition of $H_2O_2$ (Fig. 3E to H), with the effect being most marked in cultures grown at the lowest dilution rate (Fig. 3E and F).

**Differential protein expression levels in Fe-limited and Fe-replete cultures.** A total of 506 proteins from Fe-limited cultures and 323 proteins from Fe-replete cultures were identified, corresponding to proteome coverage rates of 9.7% and 6.2%, respectively. Proteins were categorized into functional groups according to CyanoBase (see Fig. S2 in the supplemental material), where the majority of identified proteins belonged to the transcriptional and translational functional group (Fe-limited cultures, 16.6%; Fe-replete cultures, 19.8%) and the energy metabolism functional group (Fe-limited cultures, 14.0%; Fe-replete cultures, 14.9%). There were large proportions of the identified proteomes (Fe-limited cultures, 26%; Fe-replete cultures, 22%) that grouped to hypothetical proteins or proteins with unknown function.

Under Fe-limited conditions, there were a total of 145 proteins that were significantly differentially regulated relative to the highest dilution (or specific growth) rate (0.45 $day^{-1}$), with 32, 107, and 78 changes observed in cultures grown at dilution rates of 0.30 $day^{-1}$, 0.15 $day^{-1}$, and 0.07 $day^{-1}$, respectively (Fig. 4; see also Table S5 in the supplemental material). Under Fe-replete conditions, only 13 proteins were differentially regulated in cultures grown at different dilution rates (Fig. 4; see also Table S6), with 3, 6, and 8 changes observed in cultures grown at dilution rates of 0.30 $day^{-1}$, 0.15 $day^{-1}$, and 0.07 $day^{-1}$, respectively. Proteins that displayed a change in abundance within Fe-replete conditions belonged solely to the energy metabolism and transport categories. However, changes in the abundance of these proteins are more likely to be associated with growth or induction by other factors (such as primary nutrients and light availability) rather than with Fe availability, since Fe concentrations were high under all dilution conditions. The full description of protein changes in Fe-limited and Fe-replete chemostats is provided in Table S5 and Table S6.

**Energy metabolism proteins.** Proteins within this category are related to the general metabolic pathways that affect growth and respiration. The majority of protein changes within this category were observed in cultures grown at the lower dilution rates (0.15 $day^{-1}$ and 0.07 $day^{-1}$). Under Fe-limited conditions, proteins from photosystem I (PSI), photosystem II (PSII), and phycobilisomes were significantly downregulated in cultures grown at dilution rates that were lower than those used for the control conditions (Fig. 5; see also Table S5 in the supplemental material). Additionally, under Fe-limited conditions, carbon fixation and glycolysis proteins were mostly downregulated, with the exception of polyhydroxyalkanoate (PHA)-specific acetoacetyl-coenzyme A (CoA) reductase (PhaB) and phosphoenolpyruvate synthase (PpsA) (Fig. 4). In contrast, under Fe-replete conditions, allophycocyanin (ApcB) and ATPase (AtpD) were the only proteins downregulated, but the downregulation was observed only in cultures grown at the 0.15 $day^{-1}$ dilution rate.

**Amino acid metabolism.** Proteins within this category are involved in the regulation of amino acid metabolism. The majority of protein changes within this category were observed in Fe-limited cultures grown at the 0.15 $day^{-1}$ dilution rate (Fig. 4). Under

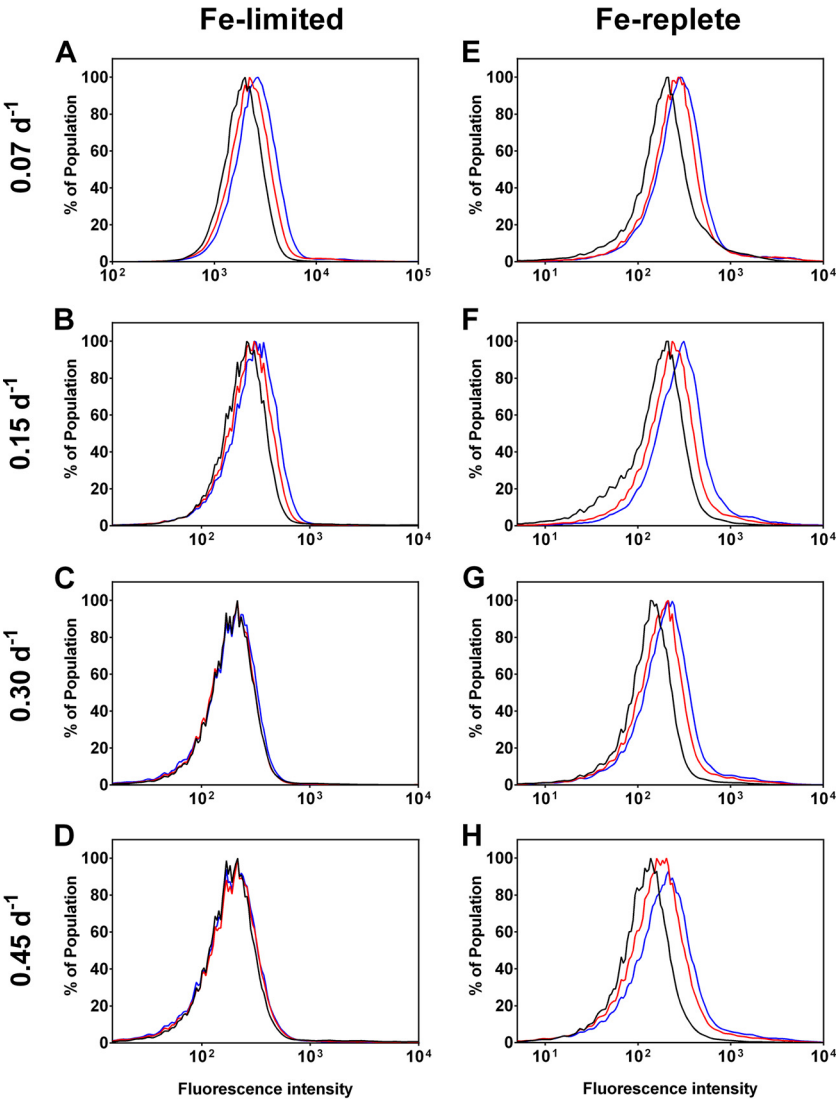


**FIG 3** Response to $H_2O_2$ in Fe-limited (left panels) and Fe-replete (right panels) chemostats. Baseline measurements ($T_0$—black line) were taken prior to induced oxidative stress. Cells were incubated with 4 mM $H_2O_2$ to induce oxidative stress, where the cellular response was measured at 10 min ($T_{10}$—red line) and 30 min ($T_{30}$—blue line) after addition. Peak shifts to the right along the *x* axis indicate increased ROS detection and hence greater oxidative stress. Sample A had the highest ROS level at $T_0$, as indicated by the right shift along the *x* axis.

these conditions, six of these proteins were upregulated by at least 2-fold, including proteins involved in aspartate, arginine, cysteine, glycine, isoleucine, and valine biosynthesis.

**Cellular processes.** Proteins within this category are involved in redox regulation. The majority of protein changes within this category were observed in Fe-limited cultures, with distinct expression profiles observed for each dilution rate. Peroxiredoxins and the universal stress protein (Usp) were downregulated in Fe-limited cultures grown at the 0.07 $day^{-1}$ dilution rate. Flavodoxin was the only protein in this category to be upregulated under the same growth conditions (Fig. 4). Fe-limited cultures grown at a dilution rate of 0.15 $day^{-1}$ had increased levels of redox reaction and oxidative stress recovery proteins, such as SOD, stationary-phase protection protein (Dps), and thioredoxin. On the other hand, cultures grown at a dilution rate of 0.30 $day^{-1}$ had increased levels of flavodoxin and decreased levels of the CBS-fused CP12 polypeptide.

**Genetic information processing—transcription and translation proteins.** The majority of proteins changes within this category were observed in Fe-limited cultures, with both 30S and 50S ribosomal subunits heavily downregulated in cultures grown at the lower dilution rates. In particular, Fe-limited cultures grown at dilution rates of 0.15 $day^{-1}$ and 0.07 $day^{-1}$ displayed the most marked reduction in ribosomal protein abundance, with many ribosomal subunits downregulated by over 3-fold. No significant changes in the expression of ribosomal proteins were observed in Fe-replete cultures (Fig. 4).

GroS chaperone and RNA-binding proteins were upregulated in Fe-limited cultures grown at the 0.15 $day^{-1}$ dilution rate, while proteases were downregulated under these conditions (Fig. 4; see also Table S5 in the supplemental material). In Fe-replete cultures grown at dilution rates of 0.07 $day^{-1}$ and 0.30 $day^{-1}$, there was a 3-fold increase in DnaK levels (Fig. 4; see also Table S6).

**Transport and binding proteins.** Proteins within this category

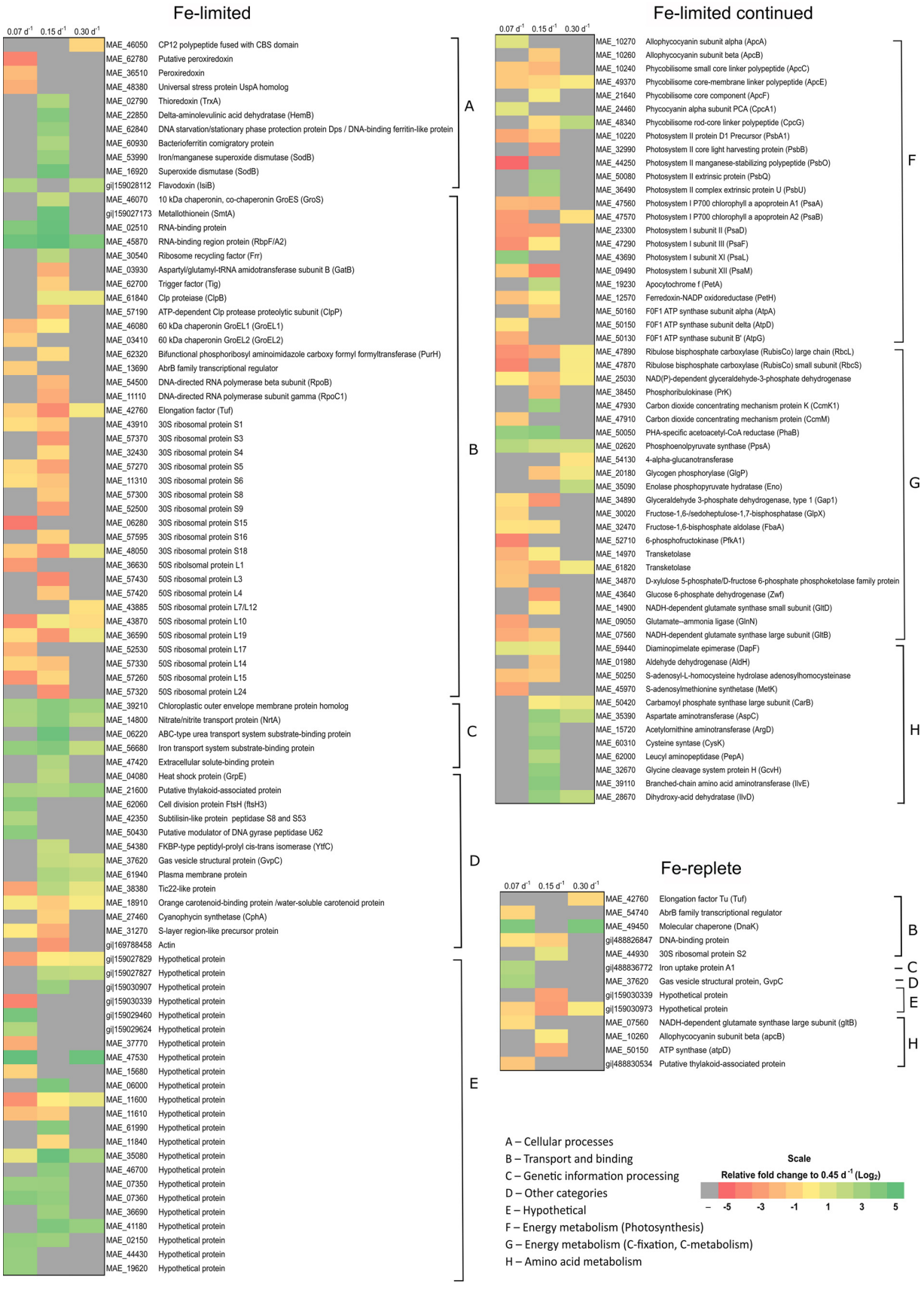


**FIG 4** Heat maps of Fe-limited and Fe-replete protein changes arranged into functional categories. Each column represents the dilution rates 0.07 day$^{-1}$, 0.15 day$^{-1}$, and 0.30 day$^{-1}$, as indicated. The scale of this heat map is given as $\log_2$ change, ranging from −5 (red) to +5 (green) relative to 0.45 day$^{-1}$. Insignificant changes in protein abundance ($P > 0.05$) are indicated in gray.

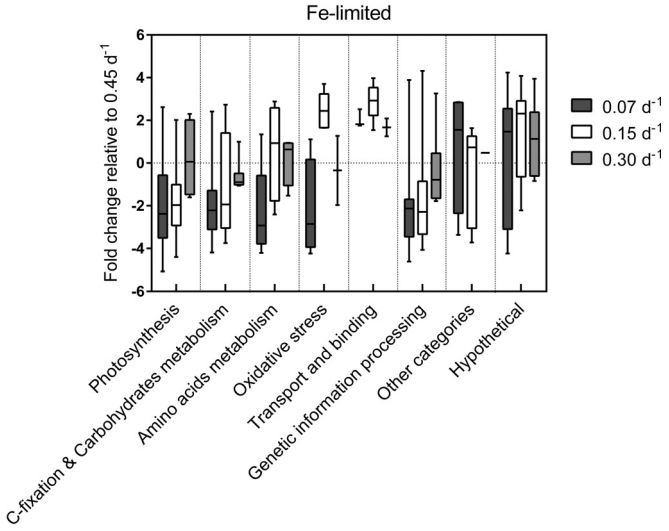


**FIG 5** Regulatory processes affected by dilution rates in Fe-limited cultures. Box plots represent the distribution of proteins with significant fold changes within each function category for each dilution rate relative to D = 0.45 day$^{-1}$. Overall placement of the box above or below 0 conveys either an increase or decrease in the abundance of proteins from that functional category, respectively. The extent of the whiskers represents the minimum and maximum fold change of the proteins in that sample.

are involved in the transport of molecules across cell membranes. The majority of protein changes within this category were observed in Fe-limited cultures, with significant upregulation occurring in cultures grown at the 0.15 day$^{-1}$ dilution rate compared to all other growth conditions (Fig. 1). As shown in Table S2 in the supplemental material, these upregulated transporter proteins included the nitrate permease (NrtA) from the nitrate/nitrite transport system (increased in abundance in all Fe-limited cultures), an ABC-type urea transporter (increased in cultures grown at the 0.15 day$^{-1}$ dilution rate), and an Fe transport protein (increased in cultures grown at the 0.15 and 0.07 day$^{-1}$ dilution rates). By comparison, the Fe uptake protein was the only transporter protein that increased in abundance in Fe-replete cultures grown at the 0.07 day$^{-1}$ dilution rate (see Table S6).

## DISCUSSION

In this study, we investigated the physiological and proteomic changes occurring in MCYST-producing *M. aeruginosa* PCC 7806 in Fe-limited and Fe-replete chemostat cultures grown at different dilution rates. Steady-state cell concentrations, determined by the balance established between the wash-out rate and the cellular growth rate in the reactor, increased with decreasing growth rates (i.e., at lower dilution rates). These observations were consistent with previous chemostat studies (31, 40) and batch culture experiments where identical Fe concentrations and media were used (data not shown). This trend resembled conventional batch culture growth curves, where low cell densities seen at high dilution rates are associated with early stages of growth, while high cell densities achieved at low dilution rates are associated with the later (stationary) stages of batch growth (41). Note that for Fe-limited chemostat cultures, the degree of Fe limitation is a function of the dilution rate. For example, cultures grown at low dilution rates experience a higher degree of Fe stress. In contrast, the degree of Fe stress in Fe-replete chemostat cultures is minimal since the overall Fe concentration remains high even in cultures grown at the lowest dilution rates. However, other nutrients, e.g., N or P or even light, may become the limiting factor in Fe-replete chemostats.

Although Chl *a* content was lower in Fe-limited cultures than in Fe-replete cultures across growth rates tested, all cultures remained green. This feature appears to be specific to the *M. aeruginosa* 7806 strain, as noted in previous *Microcystis* culturing studies (13). The increased cell size observed in cultures grown at decreasing dilution rates is consistent with the division rate in the reactor since a lower division rate means that cells have more time to grow. This result is also aligned with previous *Microcystis* studies, which suggested that cell size reflects the physiological state of the cell, where stressed cells are generally larger than unstressed cells (42, 43). However, our study results also showed decreased cell diameters in Fe-limited (i.e., Fe-stressed) cultures compared to Fe-replete cultures grown at the same dilution rate. This may have been a result of alterations in protein compositions as part of the adaptation to lower Fe availability.

**The relationship between MCYST production and growth rate changes under conditions of different Fe availabilities.** The cellular MCYST concentrations seen under Fe-limited chemostat conditions were not influenced by growth rate. These results were surprising, given that previous studies involving N-limited chemostats concluded that MCYST production was a direct function of cell growth rate (42). Interestingly, we observed an inverse relationship between cellular MCYST concentration and growth rate in Fe-replete cultures, which is consistent with batch culture findings and *in situ Microcystis* blooms, where maximum MCYST concentrations are recorded at the end of the growth cycle (i.e., lowest growth rate) or during bloom disintegration (44). The Fe-MCYST relationship observed here could have been the result of growth under favorable versus unfavorable conditions (41). For example, under Fe-replete (favorable) conditions, resources and metabolic processes are likely to be directed toward cell division. However, under Fe-limited (unfavorable) conditions, resources are diverted to pathways that increase cell fitness, such as the production of stress protection proteins and MCYST. Note that our study measured only unbound MCYST content, which may underrepresent the true total MCYST content, since membrane- and protein-bound MCYST constitutes a significant proportion of toxin within the cell (45). However, from a water quality perspective, membrane- or protein-bound MCYST is considered to be inaccessible and unable to react with hepatocytes.

**The role of MCYST in oxidative stress protection.** One of the physiological effects of Fe limitation is increased ROS generation which leads to oxidative stress (25). As discussed in detail elsewhere (31), Fe availability in our study was controlled by both the initial Fe concentration in the medium (i.e., 100 nM versus 1,000 nM) and the dilution rate at which fresh medium was replenished (i.e., 0.07 day$^{-1}$, 0.15 day$^{-1}$, 0.30 day$^{-1}$, or 0.45 day$^{-1}$). Increased ROS production was observed in Fe-limited cultures and, to a lesser extent, in Fe-replete cultures grown at the lower dilution rates. The high MCYST quota in Fe-limited cultures compared to Fe-replete cultures may provide a partial explanation for their different responses to added $H_2O_2$. The *in vitro* binding of MCYST to intracellular proteins reported by Zilliges et al. (12) suggested a functional role in protecting proteins from oxidative damage. In agreement with this, we observed that Fe-limited cultures were more resistant to $H_2O_2$ than Fe-replete cultures grown at dilution rates where $Q_{MCYST}$ levels were significantly higher. These results

suggest that MCYST may indeed protect cells against oxidative stress. Interestingly, our study revealed that there is a limit to the degree of oxidative stress protection afforded by MCYST, with cultures grown at low dilution rates (0.30 $day^{-1}$ and 0.45 $day^{-1}$) displaying increased DCF fluorescence despite having high $MCYST_{int}$ quotas. Overall, these results suggest that MCYST plays a role in protecting cells against oxidative stress; however, the importance of alternate ROS defense mechanisms should not be discounted.

**The putative function of extracellular MCYST.** In this study, extracellular MCYST was observed only in Fe-limited cultures. Microscopic inspection of cells throughout the experiment showed that they remained intact (data not shown), suggesting that an active transport pathway is responsible for the export of MCYST under these conditions. This hypothesis is in line with the observed upregulation of transporter proteins in Fe-limited cultures.

Although $MCYST_{ext}$ usually comprises only a small proportion of the total $Q_{MCYST}$ level (this study and references 6, 42, and 46), its presence in unlysed cultures suggests a possible extracellular role for the toxin. Several studies have proposed that MCYST may function as a siderophore (47, 48); however, its weak affinity for Fe renders it an unlikely candidate for Fe acquisition (49). Alternatively, MCYST might play a role in colony formation by regulating polysaccharide biosynthesis genes (50). The potential role of MCYST in allelopathy was recently examined by Phelan and Downing (51), who observed that exogenous MCYST taken up by nontoxic *Synechocystis* cells resulted in impaired PSII activity in the thylakoid membrane. Microcystin released from the cell may also act as a signaling molecule triggering MCYST production in surrounding cells and enhancing the overall fitness of the colony and greater bloom population (52), although $MCYST_{ext}$ levels are typically highest following cell lysis and bloom collapse (6, 53). In light of our results and previous reports in the literature, we propose that $MCYST_{ext}$ is likely to function as a signaling molecule which stimulates the production of $MCYST_{int}$, which, in turn, provides increased protection against ROS under conditions of Fe limitation. The allelopathic activity of MCYST is likely to be a fortuitous secondary function.

**Global proteomic and physiological responses to Fe limitation at different growth rates.** Past studies on *Synechocystis* have revealed that elements such as copper and iron can alter the expression of primary metabolism proteins as well as the expression of general stress proteins such as proteases, chaperones, and sigma factors (54). Recent studies on *Synechocystis* and *Anabaena* have demonstrated that iron limitation leads to the expression of the iron stress-induced protein (IsiA) and flavodoxin (IsiB), which act to protect and support the cyanobacterial photosystem (23, 55). Although our study identified IsiA in the Fe-limited core proteome, we did not observe any significant changes in the abundance of this protein across the different dilution rates. We therefore conclude that IsiA expression in *M. aeruginosa* PCC 7806 is a response to Fe limitation and not a function of growth rate. Unsurprisingly, the IsiA protein was not identified in the Fe-replete core proteome.

In order to alleviate the damaging effects of Fe limitation, photosynthetic organisms activate flavodoxin proteins as an electron carrier substitute for the more Fe-rich ferredoxin (56). In line with this, we observed the downregulation of ferredoxin proteins and upregulation of flavodoxin proteins in our Fe-limited chemostats. Similar results have been observed for previous Fe-limited batch cultures during late-log to early-stationary-growth phases (57).

In Fe-limited chemostats, the largest number of proteomic changes occurred in cultures grown at the lower dilution rates, which mimic the conditions of late-growth-phase batch cultures. We recorded a significant reduction in the abundance of photosynthetic proteins, including pigment and light-harvesting proteins, in these cultures compared to Fe-limited cultures grown at higher dilution rates (see Table S5 in the supplemental material).

Thylakoid membrane remodeling is quite common during cell growth and acclimation to the environment (58). In agreement with this, we observed a reduction in PSII protein expression in Fe-limited cultures grown at low dilution rates together with reductions in cellular Chl *a* concentrations as well as cell density (Table 1). The downregulation of photosynthesis proteins and pigments under conditions of Fe limitation has a negative impact on energy metabolism due to the reduction in light absorption (59).

Iron stress also has an indirect effect on growth, as levels of RuBisCO and glucose 6-phosphate proteins, which form an integral part of the glycolysis pathway, are reduced under Fe-limiting conditions (56). We also observed this phenomenon in Fe-limited *M. aeruginosa* chemostats. A reduction in levels of GroEL chaperonin proteins is likely to affect the folding of RuBisCO since the assembly process is dependent on these chaperones (60). Taken together, these processes are likely to affect cell growth and proliferation in chemostats in a manner comparable to the physiological changes observed in batch cultures of *M. aeruginosa* under conditions of Fe and N limitation (13, 22).

The majority of ribosomal proteins were downregulated in our Fe-limited cultures as previously observed in *Synechocystis* cells under conditions of N, P, or Fe depletion (61). However, RNA-binding proteins were upregulated under the same conditions. These results suggest that energy resources are directed toward the stabilization of mRNA transcripts or some other form of posttranscriptional control rather than to the synthesis of new proteins (62, 63).

Under nutrient-replete conditions, proteins for nitrogen and carbon assimilation generally follow the same pattern of regulation, since these pathways are tightly coordinated (59); that is, they decline when N and C concentrations are depleted. This was also observed in our Fe-limited chemostat cultures as they underwent metabolic shutdown (see Table S5 in the supplemental material). The downregulation of photosystem- and respiration-related proteins under conditions of Fe limitation reduced the overall growth of the cultures compared to that of their Fe-replete counterparts. These general housekeeping responses have been well documented in other cyanobacterial studies in which the effects of light stress and nutrient limitation were examined (64, 65).

*Microcystis aeruginosa* chemostat cultures also responded to Fe limitation by upregulating the expression of transporter proteins, with this response likely to lead to increased import and export of molecules across cell membranes as needed to sustain the cell. Interestingly, in this study we observed the upregulation of N and Fe transporters in Fe-limited cultures, suggesting that these two nutrients interact and coregulate photosynthesis, transcriptional regulation, and redox control pathways in *M. aeruginosa* as they do in *Anabaena* (66).

The observed presence of $MCYST_{ext}$ in Fe-limited but not Fe-replete cultures suggests the activation of a toxin export pathway

under conditions of Fe limitation. However, we did not identify changes in the expression of the putative MCYST ABC transporter, McyH (67). Interestingly, Fe-limited cultures grown at a dilution rate of 0.15 $day^{-1}$ had the highest level of $MCYST_{ext}$ as well as the greatest overall increase in the levels of transporter proteins. These results suggest that an alternative active transport pathway for the toxin may exist under certain growth conditions. While there are presently no MCYST transporter candidates aside from McyH, this is an interesting topic for future research. An alternative explanation for the high levels of $MCYST_{ext}$ observed in Fe-limited cultures relates to increased expression of the nitrate transporter (NrtA) under these conditions. Upregulation of NrtA is likely to raise the intracellular levels of nitrate and nitrite, which could then be converted into peroxynitrite via nitrate reductase (68). This reactive species could have damaging effects on the cell membrane, as well on as the photosystem (69), thus possibly contributing to passive MCYST export.

In the present study, we used continuous cultures to examine the physiological and proteomic changes in *M. aeruginosa* PCC 7806 occurring under Fe-limited and Fe-replete conditions over a range of growth rates. Unexpectedly, MCYST production was found to be growth rate dependent under Fe-replete but not Fe-limited conditions. This phenomenon may have contributed to the observed differences in the oxidative stress responses of our cultures. More importantly, we observed $MCYST_{ext}$ only in Fe-limited cultures. Under these conditions, transporter proteins were also upregulated, suggesting that the toxin is actively transported across the membrane and may have an extracellular role under conditions of Fe limitation. Although the extracellular role of MCYST is unclear, we propose that the toxin is involved in signaling surrounding cells to increase MCYST production under stressed conditions in order to enhance the fitness of the cyanobacterial colony and overall bloom population.

## ACKNOWLEDGMENTS

Anna Yeung was supported by an Australian Postgraduate Award and Water Research Australia top-up scholarship.

Helpful comments provided on a penultimate version of the manuscript by Ralitza Alexova, Manabu Fujii, and Philip Orr are gratefully appreciated. We thank Leanne Pearson for reading and editing the manuscript.

## FUNDING INFORMATION

This work, including the efforts of Brett A. Neilan, T. David Waite, Mark Bligh, Paul Michael D'Agostino, Anna C. Y. Yeung, Anne Poljak, and James McDonald, was funded by Australian Research Council Linkage Project (LP0883561). This work, including the efforts of Brett A. Neilan, T. David Waite, Mark Bligh, Anna C. Y. Yeung, and James McDonald, was funded by Water Research Australia Project (1009-09).

## REFERENCES

1. **Codd GA, Morrison LF, Metcalf JS.** 2005. Cyanobacterial toxins: risk management for health protection. Toxicol Appl Pharmacol **203:**264–272. http://dx.doi.org/10.1016/j.taap.2004.02.016.
2. **Baptista MS, Vasconcelos MT.** 2006. Cyanobacteria metal interactions: requirements, toxicity, and ecological implications. Crit Rev Microbiol **32:**127–137. http://dx.doi.org/10.1080/10408410600822934.
3. **Paerl HW, Huisman J.** 2009. Climate change: a catalyst for global expansion of harmful cyanobacterial blooms. Environ Microbiol Rep **1:**27–37. http://dx.doi.org/10.1111/j.1758-2229.2008.00004.x.
4. **Carmichael WW.** 2001. Health effects of toxin-producing cyanobacteria: "The CyanoHABs". Hum Ecol Risk Assess **7:**1393–1407. http://dx.doi.org/10.1080/20018091095087.
5. **Falconer IR.** 2005. Is there a human health hazard from microcystins in the drinking water supply? Acta Hydrochim Hydrobiol **33:**64–71. http://dx.doi.org/10.1002/aheh.200300551.
6. **Orr PT, Jones GJ.** 1998. Relationship between microcystin production and cell division rates in nitrogen-limited *Microcystis aeruginosa* cultures. Limnol Oceanogr **43:**1604–1614. http://dx.doi.org/10.4319/lo.1998.43.7.1604.
7. **Kaebernick M, Neilan BA, Borner T, Dittmann E.** 2000. Light and the transcriptional response of the microcystin biosynthesis gene cluster. Appl Environ Microbiol **66:**3387–3392. http://dx.doi.org/10.1128/AEM.66.8.3387-3392.2000.
8. **Ame MV, Wunderlin DA.** 2005. Effects of iron, ammonium and temperature on microcystin content by a natural concentrated *Microcystis aeruginosa* population. Water Air Soil Pollut **168:**235–248. http://dx.doi.org/10.1007/s11270-005-1774-8.
9. **Dziallas C, Grossart HP.** 2011. Increasing oxygen radicals and water temperature select for toxic *Microcystis* sp. PLoS One **6:**e25569. http://dx.doi.org/10.1371/journal.pone.0025569.
10. **Ginn HP, Pearson LA, Neilan BA.** 2009. Hepatotoxin biosynthesis and regulation in cyanobacteria—the putative involvement of nitrogen and iron homeostasis mechanisms. Chiang Mai J Sci **36:**200–223.
11. **Neilan BA, Pearson LA, Muenchhoff J, Moffitt MC, Dittmann E.** 2013. Environmental conditions that influence toxin biosynthesis in cyanobacteria. Environ Microbiol **15:**1239–1253. http://dx.doi.org/10.1111/j.1462-2920.2012.02729.x.
12. **Zilliges Y, Kehr JC, Meissner S, Ishida K, Mikkat S, Hagemann M, Kaplan A, Borner T, Dittmann E.** 2011. The cyanobacterial hepatotoxin microcystin binds to proteins and increases the fitness of *Microcystis* under oxidative stress conditions. PLoS One **6:**e17615. http://dx.doi.org/10.1371/journal.pone.0017615.
13. **Alexova R, Fujii M, Birch D, Cheng J, Waite TD, Ferrari BC, Neilan BA.** 2011. Iron uptake and toxin synthesis in the bloom-forming *Microcystis aeruginosa* under iron limitation. Environ Microbiol **13:**1064–1077. http://dx.doi.org/10.1111/j.1462-2920.2010.02412.x.
14. **Nagai T, Imai A, Matsushige K, Yokoi K, Fukushima T.** 2007. Dissolved iron and its speciation in a shallow eutrophic lake and its inflowing rivers. Water Res **41:**775–784. http://dx.doi.org/10.1016/j.watres.2006.10.038.
15. **Anderson MA, Morel FMM.** 1982. The influence of aqueous iron chemistry on the uptake of iron by the coastal diatom *Thalassiosira weisflogii*. Limnol Oceanogr **27:**789–813. http://dx.doi.org/10.4319/lo.1982.27.5.0789.
16. **Imai A, Fukushima T, Matsushige K.** 1999. Effects of iron limitation and aquatic humic substances on the growth of *Microcystis aeruginosa*. Can J Fish Aquat Sci **56:**1929–1937. http://dx.doi.org/10.1139/f99-131.
17. **Keren N, Aurora R, Pakrasi HB.** 2004. Critical roles of bacterioferritins in iron storage and proliferation of cyanobacteria. Plant Physiol **135:**1666–1673. http://dx.doi.org/10.1104/pp.104.042770.
18. **Ferreira F, Straus NA.** 1994. Iron deprivation in cyanobacteria. J Appl Phycol **6:**199–210. http://dx.doi.org/10.1007/BF02186073.
19. **Xing W, Liu GH.** 2011. Iron biogeochemistry and its environmental impacts in freshwater lakes. Fresenius Environ Bull **20:**1339–1345.
20. **Shcolnick S, Keren N.** 2006. Metal homeostasis in cyanobacteria and chloroplasts. Balancing benefits and risks to the photosynthetic apparatus. Plant Physiol **141:**805–810.
21. **Schrader PS, Milligan AJ, Behrenfeld MJ.** 2011. Surplus photosynthetic antennae complexes underlie diagnostics of iron limitation in a cyanobacterium. PLoS One **6:**e18753. http://dx.doi.org/10.1371/journal.pone.0018753.
22. **Alexova R, Dang TC, Fujii M, Raftery MJ, Waite TD, Ferrari BC, Neilan BA.** 2016. Specific global responses to N and Fe nutrition in toxic and non-toxic *Microcystis aeruginosa*. Environ Microbiol **18:**401–413. http://dx.doi.org/10.1111/1462-2920.12958.
23. **Latifi A, Jeanjean R, Lemeille S, Havaux M, Zhang CC.** 2005. Iron starvation leads to oxidative stress in *Anabaena* sp. strain PCC 7120. J Bacteriol **187:**6596–6598. http://dx.doi.org/10.1128/JB.187.18.6596-6598.2005.
24. **Yingping F, Lemeille S, Talla E, Janicki A, Denis Y, Zhang CC, Latifi A.** 2014. Unravelling the cross-talk between iron starvation and oxidative stress responses highlights the key role of PerR (alr0957) in peroxide signalling in the cyanobacterium *Nostoc* PCC 7120. Environ Microbiol Rep **6:**468–475. http://dx.doi.org/10.1111/1758-2229.12157.
25. **Latifi A, Ruiz M, Zhang CC.** 2009. Oxidative stress in cyanobacteria. FEMS Microbiol Rev **33:**258–278. http://dx.doi.org/10.1111/j.1574-6976.2008.00134.x.
26. **Rivers AR, Jakuba RW, Webb EA.** 2009. Iron stress genes in marine

*Synechococcus* and the development of a flow cytometric iron stress assay. Environ Microbiol **11:**382–396. http://dx.doi.org/10.1111/j.1462-2920.2008.01778.x.
27. **Imlay JA.** 2003. Pathways of oxidative damage. Annu Rev Microbiol **57:**395–418. http://dx.doi.org/10.1146/annurev.micro.57.030502.090938.
28. **Song W, Xu T, Cooper WJ, Dionysiou DD, de la Cruz AA, O'Shea KE.** 2009. Radiolysis studies on the destruction of microcystin-LR in aqueous solution by hydroxyl radicals. Environ Sci Technol **43:**1487–1492. http://dx.doi.org/10.1021/es802282n.
29. **Antoniou MG, de la Cruz AA, Dionysiou DD.** 2010. Intermediates and reaction pathways from the degradation of microcystin-LR with sulfate radicals. Environ Sci Technol **44:**7238–7244. http://dx.doi.org/10.1021/es1000243.
30. **Anderson RA.** 2005. Algal culturing techniques. Academic Press, Burlington, MA.
31. **Dang TC, Fujii M, Rose AL, Bligh M, Waite TD.** 2012. Characteristics of the freshwater cyanobacterium *Microcystis aeruginosa* grown in iron-limited continuous culture. Appl Environ Microbiol **78:**1574–1583. http://dx.doi.org/10.1128/AEM.06908-11.
32. **Meeks JC, Castenholz RW.** 1971. Growth and photosynthesis in an extreme thermophile, *Synechococcus lividus* (Cyanophyta). Arch Mikrobiol **78:**25–41. http://dx.doi.org/10.1007/BF00409086.
33. **Rastogi RP, Singh SP, Haider D-P, Sinha RP.** 2010. Detection of reactive oxygen species (ROS) by the oxidant-sensing probe 2′,7′-dichlorodihydrofluorescein diacetate in the cyanobacterium *Anabaena variabilis* PCC 7939. Biochem Biophys Res Commun **397:**603–607. http://dx.doi.org/10.1016/j.bbrc.2010.06.006.
34. **Battchikova N, Vainonen JP, Vorontsova N, Keranen M, Carmel D, Aro EM.** 2010. Dynamic changes in the proteome of *Synechocystis* 6803 in response to $CO_2$ limitation revealed by quantitative proteomics. J Proteome Res **9:**5896–5912. http://dx.doi.org/10.1021/pr100651w.
35. **Dyballa N, Metzger S.** 2009. Fast and sensitive colloidal Coomassie G-250 staining for proteins in polyacrylamide gels. J Vis Exp **2009:**1431. http://dx.doi.org/10.3791/1431.
36. **Williams TJ, Burg DW, Ertan H, Raftery MJ, Poljak A, Guilhaus M, Cavicchioli R.** 2010. Global proteomic analysis of the insoluble, soluble, and supernatant fractions of the psychrophilic archaeon *Methanococcoides burtonii*. Part II: the effect of different methylated growth substrates. J Proteome Res **9:**653–663. http://dx.doi.org/10.1021/pr9005102.
37. **Gatlin CL, Kleemann GR, Hays LG, Link AJ, Yates JR.** 1998. Protein identification at the low femtomole level from silver-stained gels using a new fritless electrospray interface for liquid chromatography-microspray and nanospray mass spectrometry. Anal Biochem **263:**93–101. http://dx.doi.org/10.1006/abio.1998.2809.
38. **Vizcaino J, Deutsch E, Wang R, Csordas A, Reisinger F, Rios D, Dianes J, Sun Z, Farrah T, Bandeira N, Binz P, Xenarios I, Elsenacher M, Mayer G, Gatto L, Campos A, Chalkley R, Kraus H, Albar J, Martinez-Bartolome S, Apweiler R, Omenn GS, Martens L, Jones A, Hermjakob H.** 2014. ProteomeXchange provides globally co-ordinated proteomics data submission and dissemination. Nat Biotechnol **30:**223–226. http://dx.doi.org/10.1038/nbt.2839.
39. **Tonk L, Welker M, Huisman J, Visser PM.** 2009. Production of cyanopeptolins, anabaenopeptins, and microcystins by the harmful cyanobacteria *Anabaena* 90 and *Microcystis* PCC 7806. Harmful Algae **8:**219–224. http://dx.doi.org/10.1016/j.hal.2008.05.005.
40. **Oh HM, Lee SJ, Jang MH, Yoon BD.** 2000. Microcystin production by *Microcystis aeruginosa* in a phosphorus-limited chemostat. Appl Environ Microbiol **66:**176–179. http://dx.doi.org/10.1128/AEM.66.1.176-179.2000.
41. **Lyck S.** 2004. Simultaneous changes in cell quotas of microcystin, chlorophyll a, protein and carbohydrate during different growth phases of a batch culture experiment with *Microcystis aeruginosa*. J Plankton Res **26:**727–736. http://dx.doi.org/10.1093/plankt/fbh071.
42. **Long BM, Jones GJ, Orr PT.** 2001. Cellular microcystin content in N-limited *Microcystis aeruginosa* can be predicted from growth rate. Appl Environ Microbiol **67:**278–283. http://dx.doi.org/10.1128/AEM.67.1.278-283.2001.
43. **Krüger GHJ, Eloff JN.** 1981. The effect of physico-chemical factors on growth relevant to the mass culture of axenic *Microcystis*, p 193–222. *In* Carmichael WW (ed), The water environment: algal toxins and health. Springer US, Boston, MA. http://dx.doi.org/10.1007/978-1-4613-3267-1_15.
44. **Shirai M, Ohtake A, Sano T, Matsumoto S, Sakamoto T, Sato A, Aida T, Harada K, Shimada T, Suzuki M, Nakano M.** 1991. Toxicity and toxins of natural blooms and isolated strains of *Microcystis* spp. (Cyanobacteria) and improved procedure for purification of cultures. Appl Environ Microbiol **57:**1241–1245.
45. **Meissner S, Fastner J, Dittmann E.** 2013. Microcystin production revisited: conjugate formation makes a major contribution. Environ Microbiol **15:**1810–1820. http://dx.doi.org/10.1111/1462-2920.12072.
46. **Wiedner C, Visser PM, Fastner J, Metcalf JS, Codd GA, Mur LR.** 2003. Effects of light on the microcystin content of *Microcystis* strain PCC 7806. Appl Environ Microbiol **69:**1475–1481. http://dx.doi.org/10.1128/AEM.69.3.1475-1481.2003.
47. **Shi L, Carmichael WW, Miller I.** 1995. Immuno-gold localization of hepatotoxins in cyanobacterial cells. Arch Microbiol **163:**7–15. http://dx.doi.org/10.1007/BF00262197.
48. **Utkilen H, Gjolme N.** 1995. Iron-stimulated toxin production in *Microcystis aeruginosa*. Appl Environ Microbiol **61:**797–800.
49. **Klein AR, Baldwin DS, Silvester E.** 2013. Proton and iron binding by the cyanobacterial toxin microcystin-LR. Environ Sci Technol **47:**5178–5184. http://dx.doi.org/10.1021/es400464e.
50. **Gan N, Xiao Y, Zhu L, Wu Z, Liu J, Hu C, Song L.** 2012. The role of microcystins in maintaining colonies of bloom-forming *Microcystis* spp. Environ Microbiol **14:**730–742. http://dx.doi.org/10.1111/j.1462-2920.2011.02624.x.
51. **Phelan RR, Downing TG.** 2014. The localization of exogenous microcystin LR taken up by a non-microcystin producing cyanobacterium. Toxicon **89:**87–90. http://dx.doi.org/10.1016/j.toxicon.2014.07.007.
52. **Schatz D, Keren Y, Vardi A, Sukenik A, Carmeli S, Borner T, Dittmann E, Kaplan A.** 2007. Towards clarification of the biological role of microcystins, a family of cyanobacterial toxins. Environ Microbiol **9:**965–970. http://dx.doi.org/10.1111/j.1462-2920.2006.01218.x.
53. **Li HL, Murphy T, Guo J, Parr T, Nalewajko C.** 2009. Iron-stimulated growth and microcystin production of *Microcystis novacekii* UAM 250. Limnologica **39:**255–259. http://dx.doi.org/10.1016/j.limno.2008.08.002.
54. **Castielli O, De la Cerda B, Navarro JA, Hervás M, De la Rosa MA.** 2009. Proteomic analyses of the response of cyanobacteria to different stress conditions. FEBS Lett **583:**1753–1758. http://dx.doi.org/10.1016/j.febslet.2009.03.069.
55. **Hernández-Prieto MA, Schön V, Georg J, Barreira L, Varela J, Hess WR, Futschik ME.** 2012. Iron deprivation in *Synechocystis*: inference of pathways, non-coding RNAs, and regulatory elements from comprehensive expression profiling. G3 (Bethesda) **2:**1475–1495. http://dx.doi.org/10.1534/g3.112.003863.
56. **Fromme P, Melkozernov A, Jordan P, Krauss N.** 2003. Structure and function of photosystem I: interaction with its soluble electron carriers and external antenna systems. FEBS Lett **555:**40–44. http://dx.doi.org/10.1016/S0014-5793(03)01124-4.
57. **Alexova R.** 2010. The regulation of toxin synthesis in *Microcystis aeruginosa*. PhD thesis. The University of New South Wales, Sydney, Australia.
58. **Gan F, Zhang S, Rockwell NC, Martin SS, Lagarias JC, Bryant DA.** 2014. Extensive remodeling of a cyanobacterial photosynthetic apparatus in far-red light. Science **345:**1312–1317. http://dx.doi.org/10.1126/science.1256963.
59. **Wang C, Kong HN, Wang XZ, Wu HD, Lin Y, He SB.** 2010. Effects of iron on growth and intracellular chemical contents of *Microcystis aeruginosa*. Biomed Environ Sci **23:**48–52. http://dx.doi.org/10.1016/S0895-3988(10)60031-1.
60. **Liu C, Young AL, Starling-Windhof A, Bracher A, Saschenbrecker S, Rao BV, Rao KV, Berninghausen O, Mielke T, Hartl FU, Beckmann R, Hayer-Hartl M.** 2010. Coupled chaperone action in folding and assembly of hexadecameric Rubisco. Nature **463:**197–202. http://dx.doi.org/10.1038/nature08651.
61. **Wegener KM, Singh AK, Jacobs JM, Elvitigala T, Welsh EA, Keren N, Gritsenko MA, Ghosh BK, Camp DG, II, Smith RD, Pakrasi HB.** 2010. Global proteomics reveal an atypical strategy for carbon/nitrogen assimilation by a cyanobacterium under diverse environmental perturbations. Mol Cell Proteomics **9:**2678–2689. http://dx.doi.org/10.1074/mcp.M110.000109.
62. **Takayama K, Kjelleberg S.** 2000. The role of RNA stability during bacterial stress responses and starvation. Environ Microbiol **2:**355–365. http://dx.doi.org/10.1046/j.1462-2920.2000.00119.x.
63. **Dressaire C, Picard F, Redon E, Loubière P, Queinnec I, Girbal L, Cocaign-Bousquet M.** 2013. Role of mRNA stability during bacterial adaptation. PLoS One **8:**e59059. http://dx.doi.org/10.1371/journal.pone.0059059.
64. **Pandhal J, Wright PC, Biggs CA.** 2007. A quantitative proteomic analysis

of light adaptation in a globally significant marine cyanobacterium *Prochlorococcus marinus* MED4. J Proteome Res **6:**996–1005. http://dx.doi.org/10.1021/pr060460c.

65. **Xing W, Huang WM, Liu GH, Liu YD.** 2008. Effects of iron on physiological and biochemical characteristics of *Microcystis wesenbergii* (Kom.) Kom. (Cyanobacterium). Fresenius Environ Bull **17:**2034–2042.
66. **López-Gomollón S, Hernández JA, Pellicer S, Angarica VE, Peleato ML, Fillat MF.** 2007. Cross-talk between iron and nitrogen regulatory networks in *Anabaena* (*Nostoc*) sp. PCC 7120: identification of overlapping genes in FurA and NtcA regulons. J Mol Biol **374:**267–281. http://dx.doi.org/10.1016/j.jmb.2007.09.010.
67. **Pearson LA, Hisbergues M, Borner T, Dittmann E, Neilan BA.** 2004. Inactivation of an ABC transporter gene, *mcyH*, results in loss of microcystin production in the cyanobacterium *Microcystis aeruginosa* PCC 7806. Appl Environ Microbiol **70:**6370–6378. http://dx.doi.org/10.1128/AEM.70.11.6370-6378.2004.
68. **Chen WM, Zhang QM, Dai SG.** 2009. Effects of nitrate on intracellular nitrite and growth of *Microcystis aeruginosa*. J Appl Phycol **21:**701–706. http://dx.doi.org/10.1007/s10811-009-9405-1.
69. **Chen WM, Liu H.** 2015. Intracellular nitrite accumulation: The cause of growth inhibition of *Microcystis aeruginosa* exposure to high nitrite level. Phycol Res **63:**197–201. http://dx.doi.org/10.1111/pre.12090.